THE JOURNAL OF BIOLOGICAL CHEMISTRY VOL. 291, NO. 35, pp. 18283–18298, August 26, 2016

Parkinson Disease-linked Vps35 R524W Mutation Impairs the Endosomal Association of Retromer and Induces α-Synuclein Aggregation*

Received for publication, November 10, 2015, and in revised form, June 26, 2016 Published, JBC Papers in Press, July 6, 2016, DOI 10.1074/jbc.M115.703157

Jordan Follett[‡], Andrea Bugarcic[‡], Zhe Yang[‡], Nicholas Ariotti[‡], Suzanne J. Norwood[‡], Brett M. Collins[‡1], Robert G. Parton[‡§2], and Rohan D. Teasdale[‡3]

From the [‡]Institute for Molecular Bioscience, University of Queensland, St. Lucia, Queensland 4072, Australia and the [§]Centre for Microscopy and Microanalysis, University of Queensland, Brisbane, Queensland 4072, Australia

Endosomal sorting is a highly orchestrated cellular process. Retromer is a heterotrimeric complex that associates with endosomal membranes and facilitates the retrograde sorting of multiple receptors, including the cation-independent mannose 6-phosphate receptor for lysosomal enzymes. The cycling of retromer on and off the endosomal membrane is regulated by a network of retromer-interacting proteins. Here, we find that Parkinson disease-associated Vps35 variant, R524W, but not P316S, is a loss-of-function mutation as marked by a reduced association with this regulatory network and dysregulation of endosomal receptor sorting. Expression of Vps35 R524W-containing retromer results in the accumulation of intracellular α-synuclein-positive aggregates, a hallmark of Parkinson disease. Overall, the Vps35 R524W-containing retromer has a decreased endosomal association, which can be partially rescued by R55, a small molecule previously shown to stabilize the retromer complex, supporting the potential for future targeting of the retromer complex in the treatment of Parkinson disease.

Parkinson disease (PD)[4] primarily affects the dopaminergic neurons of the substantia nigra pars compacta, a small anatomical region located within the midbrain that regulates movement. On a cellular level, PD is a complex disease characterized by the subcellular formation of large, perinuclear accumulations of aggregated proteins, called Lewy bodies (LBs). The most abundant protein found in LBs is the presynaptic plasma membrane-associated protein α-synuclein, but they may also contain other proteins and lipids (1–3). The formation of LBs, which individual neurons are unable to clear, has been directly linked to activation of apoptotic pathways in the dopaminergic neurons (2).

Rare familial mutations in a range of proteins have been identified and have provided significant insight into the molecular pathways involved in the manifestation of PD (reviewed in Ref. 4). Recently, a number of point mutations (D620N, P316S, R524W, and L774M) within the retromer subunit Vps35 (vacuolar protein sorting 35) were associated with late onset PD, and analysis of 144 individuals confirmed that overall levels of Vps35 mRNA in the substantia nigra were significantly decreased in PD-affected patients (5–7). Retromer is a heterotrimeric complex composed of Vps29, Vps35, and one of the two Vps26 subunits, Vps26A or Vps26B (8–10). Retromer has a central role in the sorting of receptor cargo within endosomal membranes, which is essential to coordinate the specific spatiotemporal localization of individual receptors, enabling them to perform their varied functions (11, 12). One such cargo is the cation-independent mannose 6-phosphate receptor (CI-M6PR) that controls the sorting of lysosomal enzymes, such as cathepsin D, which is required for protein turnover (11–13). Retromer serves as a multifunctional scaffold forming an interaction hub for a wide array of endosome-associated proteins, collectively termed the retromer interactome. These interactions aid in the formation of the cargo-containing tubulovesicular membrane carriers destined for other compartments, such as the Golgi apparatus and plasma membrane. The diverse proteins that associate with retromer include regulatory molecules, proteins required for membrane recruitment, and protein complexes that control membrane tubulation and scission (reviewed in Refs. 14 and 15). It is the spatial and temporal coordination of the interactions between the retromer and retromer interactome that enables it to coordinate multiple endosome-derived trafficking pathways (16).

Characterization of the PD-causing Vps35 D620N mutation demonstrated that Vps35 D620N-retromer is unable to correctly traffic cargoes, such as CI-M6PR and post-synaptic AMPA receptors, the former of which results in improper processing and trafficking of cathepsin D (17, 18). Moreover, previous reports suggest that the aforementioned sorting defect may arise from perturbed interactions with the WASH complex, a protein complex implicated in endosome-to-Golgi receptor sorting, and, consequently, may lead to a down-regu-

* This work was supported by National Health and Medical Research Council (NHMRC) of Australia Grants APP1025538, APP1037320, APP1042082, APP1045092, and APP1058734; Australian Research Council Project Grant DP120103930 and Centre of Excellence in Convergent Bio-Nano Science and Technology; and an ANZ Trustees National Medical Program Grant from the Judith Jane Mason and Harold Stannett Williams Memorial Foundation. The authors declare that they have no conflicts of interest with the contents of this article.

[1] Supported by NHMRC Career Development Fellowship APP1061574 and ARC Future Fellowship FT100100027.

[2] Supported by NHMRC Senior Principal Research Fellowship APP1058565.

[3] Supported by NHMRC Senior Research Fellowship APP1041929. To whom correspondence should be addressed. Tel.: 61-3202-9143; E-mail: r.teasdale@uq.edu.au.

[4] The abbreviations used are: PD, Parkinson disease; LB, Lewy body; TGN, *trans*-Golgi network; AEBSF, 4-(2-aminoethyl)-benzenesulfonyl fluoride; CI-M6PR, cation-independent mannose 6-phosphate receptor; ITC, isothermal titration calorimetry; APEX, ascorbate peroxidase; GBP, GFP-binding peptide; TK, thymidine kinase; ANOVA, analysis of variance.

lation of autophagy (19–21). Together, these studies support the importance of the late endocytic network in the degradation of cellular proteins and highlight the importance of a specific protease, cathepsin D, in overall lysosomal function and the degradation of luminal α-synuclein.

Here, we report the cellular characterization of two familial PD-linked Vps35 variants, Vps35 P316S and Vps35 R524W. Whereas the P316S variant appears to have little impact on retromer assembly or function, Vps35 R524W is poorly recruited to endosomes and impairs the recruitment of retromer-dependent interacting proteins and the trafficking of CI-M6PR. Similar to that observed for Vps35 D620N, expression of Vps35 R524W induced higher levels of α-synuclein-positive aggregates when compared with that of Vps35 WT or Vps35 P316S. These findings provide insight into the underlying molecular mechanism of PD-linked Vps35 R524W and retromer's involvement in the molecular pathways associated with PD.

Results

Vps35 P316S and Vps35 R524W Are Incorporated into Retromer Complexes—To determine whether the formation of the heterotrimeric retromer complex in the presence of Vps35 variants P316S and R524W is altered, *in vitro* isothermal titration calorimetry (ITC) and *in vivo* co-immunoprecipitation were employed using full-length recombinant Vps35 proteins and GFP fusion constructs, respectively. The arginine 524 residue is present in an exposed loop between α-helices of the reiterating pairs of HEAT-like α-helical repeats and contributes indirectly to the VPS35 interface with VPS29, as shown in the co-crystal structure (22). The proline 316 residue is predicted to be within an intervening loop, so its substitution is unlikely to disrupt the overall Vps35 structure. As demonstrated by ITC, Vps35 P316S retained interaction with retromer subunits Vps26A and Vps29 (K_d = 1.5 and 170 nM, respectively) at thermodynamic profiles similar to that of wild-type Vps35 (K_d = 1.1 and 250 nM, respectively). The Vps35 R524W mutant also demonstrated a binding affinity similar to that of the wild-type Vps35 for Vps29 (K_d = 303 nM) and Vps26A (K_d = 1.4 nM) (Fig. 1*A*). In support of these *in vitro* experiments, co-immunoprecipitation from HeLa cells transiently expressing GFP fusion constructs demonstrated that Vps35 P316S and Vps35 R524W interact with retromer subunits Vps26A and Vps29 in whole cell lysates or the cytosolic fraction (Fig. 1, *B* and *C*). The incorporation of the PD-associated variants of Vps35 into Vps26A-retromer complexes was confirmed by co-immunoprecipitation of endogenous Vps26A (Fig. 1*D*). Collectively, these data demonstrate that both PD-associated mutations can form stable retromer trimers, and their expression does not alter steady state protein levels of endogenous retromer subunits. However, comparison of the relative amounts of the retromer subunits co-precipitated indicates that a portion of Vps35 R524W does not appear to be complexed to Vps26A and Vps29.

Vps35 R524W-containing Retromer Has Diminished Endosome Recruitment—The subcellular localization of Vps35 P316S and Vps35 R524W was determined in HeLa cells transiently expressing Vps35 WT-GFP, Vps35 P316S-GFP, or Vps35 R524W-GFP. Consistent with the subcellular localization of Vps35 WT-GFP, Vps35 P316S-GFP demonstrated a high level of endosomal recruitment and displayed a high level of co-localization with Vps26A on these endosomes (Fig. 2*A*). In contrast to this, whereas Vps35 R524W-GFP showed partial endosomal recruitment, where it co-localized with Vps26A, a significant fraction of the protein also showed a diffuse localization to the cytosol (Fig. 2*A*).

Membrane fractionation was employed to determine the relative proportion of retromer associated with membranes. HeLa cells transiently transfected with GFP fusion constructs were lysed in sucrose-containing buffer, and cytosolic and microsome fractions were isolated. Loading controls and purity of the fractions were monitored using late endosome marker LAMP1 (microsome) and β-tubulin (cytoplasmic). Consistent with the previously described data, wild-type retromer proteins, including Vps35 WT-GFP, were observed associated with membranes and within the cytosol. Vps35 P316S-GFP showed a distribution similar to Vps35 WT-GFP, whereas Vps35 R524W-GFP was predominantly distributed in the cytosol with a proportional decrease in the protein associated with membranes. Further, Western blotting of endogenous Vps26A, Vps35, and Vps29 demonstrated no significant shift in total levels of retromer from the microsomal fraction following expression of the GFP fusion constructs (Fig. 2*B*). The biochemical and immunofluorescence findings together suggest impaired endosome association of Vps35 R524W.

We employed confocal microscopy to further examine the endosome morphology and retromer localization in the presence of Vps35 P316S and Vps35 R524W (Fig. 2*C*). HeLa cells transiently expressing GFP fusion constructs were immunolabeled with antibodies against early endosome marker, EEA1, or late endosomal marker, LAMP1. Consistent with the expression of Vps35 WT-GFP, confocal microscopy revealed recruitment of Vps35 P316S-GFP to EEA1-positive endosomes (R_{WT} = 0.2130 and R_{P316S} = 0.2013; Fig. 2*D*), whereas cells expressing Vps35 R524W-GFP demonstrated reduced overlap with EEA1-positive compartments (R_{R524W} = 0.1551; Fig. 2*D*). However, no differences in the morphology of EEA1-positive endosomes, when compared with neighboring untransfected cells, were observed in transfected cells expressing any of the Vps35 proteins (Fig. 2*C*). Immunolabeling of HeLa cells with antibodies against LAMP1 revealed no gross morphological changes of late endosome compartments in cells expressing Vps35 WT-GFP or Vps35 P316S-GFP. In contrast, expression of Vps35 R524W induced some swelling of the late endosome but did not influence the overall localization of LAMP1-positive compartments when compared with neighboring untransfected cells (Fig. 2*C*). Further, consistent with previous observations, LAMP1 displayed minor overlap with Vps35 WT-GFP, Vps35 P316S-GFP, and Vps35 R524W-GFP (R_{WT} = 0.0330, R_{P316S} = 0.0518, and R_{R524W} = 0.0428, respectively; Fig. 2*D*).

Subcellular Localization of Vps35 Mutants Using Ascorbate Peroxidase (APEX)-GFP-binding peptide (GBP)—To resolve the redistribution of Vps35 generated by the various point mutations at a higher resolution, we utilized a modified APEX tag for characterizing subcellular protein distribution with electron microscopy. Recently, a genetically encoded plasmid

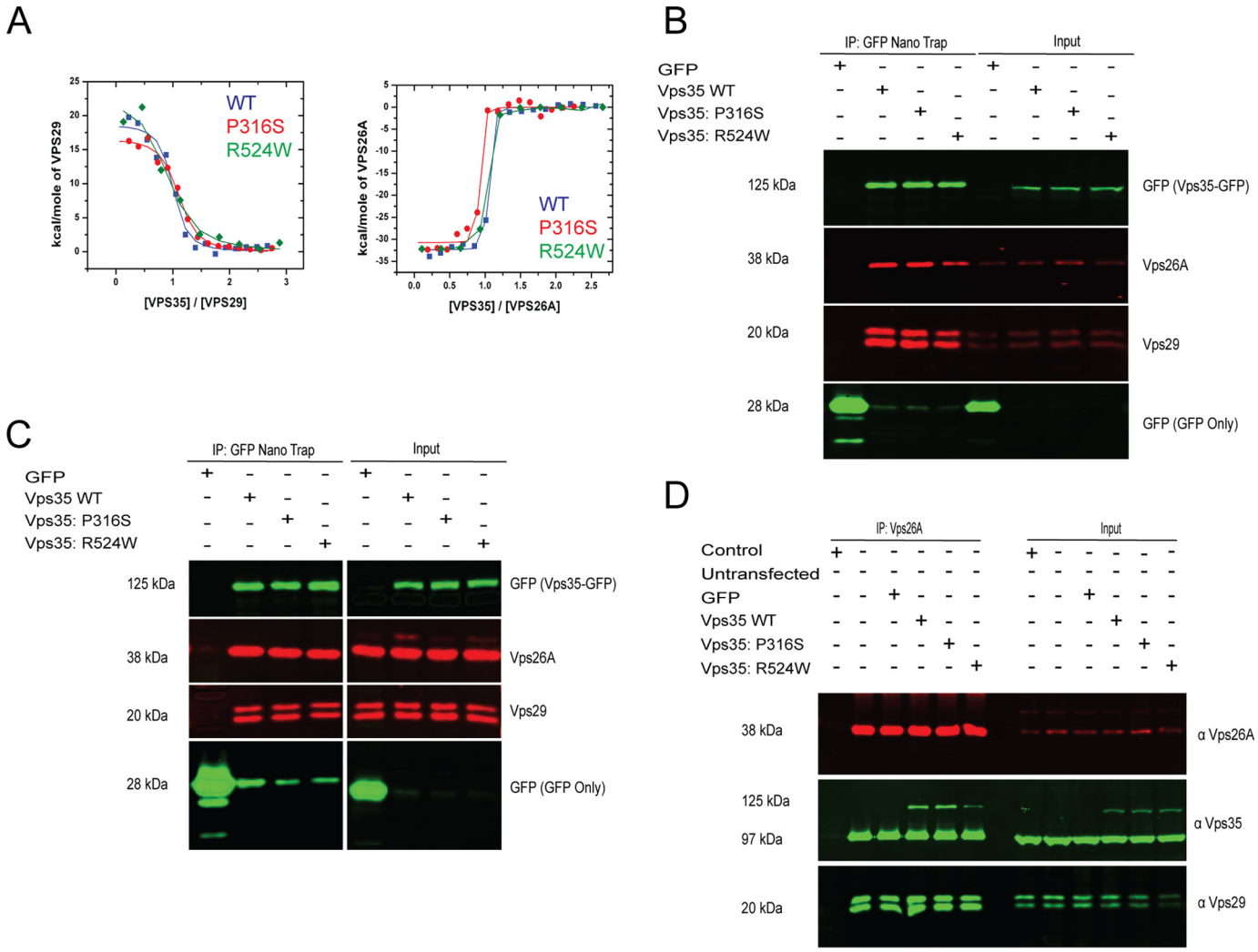

FIGURE 1. **Parkinson disease-linked Vps35 mutants P316S and R524W do not disrupt trimer formation.** *A*, isothermal titration calorimetry of Vps35 point mutations with retromer subunits, Vps29 (*left*) and Vps26A (*right*). *B* and *C*, GFP-NanoTrap immunoprecipitations from HeLa cell whole cell lysates (*B*) or cytosolic subcellular fractions (*C*) of transiently expressing GFP, Vps35 WT-GFP, Vps35 P316S-GFP, or Vps35 R524W-GFP followed by immunoblotting analysis of precipitated complexes with anti-GFP, anti-Vps26A, and anti-Vps29 antibodies. *D*, endogenous Vps26A was immunoprecipitated from HeLa cells transiently expressing GFP, Vps35 WT-GFP, Vps35 P316S-GFP, or Vps35 R524W-GFP followed by immunoblotting analysis of precipitated complexes with anti-Vps35, anti-Vps26A, and anti-Vps29 antibodies. Within the *control lane* the same experimental procedure was applied in the absence of the primary anti-Vps26A antibody.

for modular detection of any GFP-tagged protein of interest has been developed that employs co-transfection of APEX directly conjugated to a GBP (23). When APEX-GBP is expressed, it binds to the GFP-tagged protein, resulting in the formation of specific electron density at the site of the protein after the diaminobenzoic acid reaction in the presence of H_2O_2 and post-fixation with osmium tetroxide (23). Control expression of APEX-GBP alone and APEX-GBP + GFP resulted in significant electron density in the cytoplasm of transfected cells but no enriched electron density at endosomes/multivesicular bodies (Fig. 3, *A* and *B*). However, the expression of Vps35 WT-GFP with APEX-GBP resulted in specific and enriched electron density at the site of morphologically identifiable endosomes (Fig. 3*C*). Vps35 P316S-GFP was enriched at endosomes and present on the external leaflet of endosomes, analogous to the WT (Fig. 3*D*). Vps35 R524W-GFP, when co-transfected with APEX-GBP, had reduced enrichment at the cytosolic face of endosomes and an increase in the abundance of soluble reaction product (Fig. 3*E*), resembling the expression of APEX-GBP alone and GFP + APEX-GBP. As an additional positive control, we analyzed the distribution of Vps35 D620N-GFP, a point mutant that we have previously demonstrated generates an enlarged and clustered endosomal network. Strikingly, this mutant resulted in specific reaction product at enlarged and morphologically distinct endosomes and a reduction of the soluble pool of the protein (Fig. 3*F*).

The Association of Vps35 R524W with Regulators of the Retromer Complex Is Impaired—Retromer does not bind directly to membranes, and its recruitment to endosomes is controlled by its capacity to coordinate interactions with a number of membrane-associated proteins. Association of the retromer complex with the endosomal membrane is positively regulated by the small GTPase Rab7a and negatively regulated by the RabGAP TBC1D5 (24). Following recruitment to the endosome, additional retromer-dependent sorting machinery, such as the Arp2/3-activating complex, WASH, is recruited to aid in

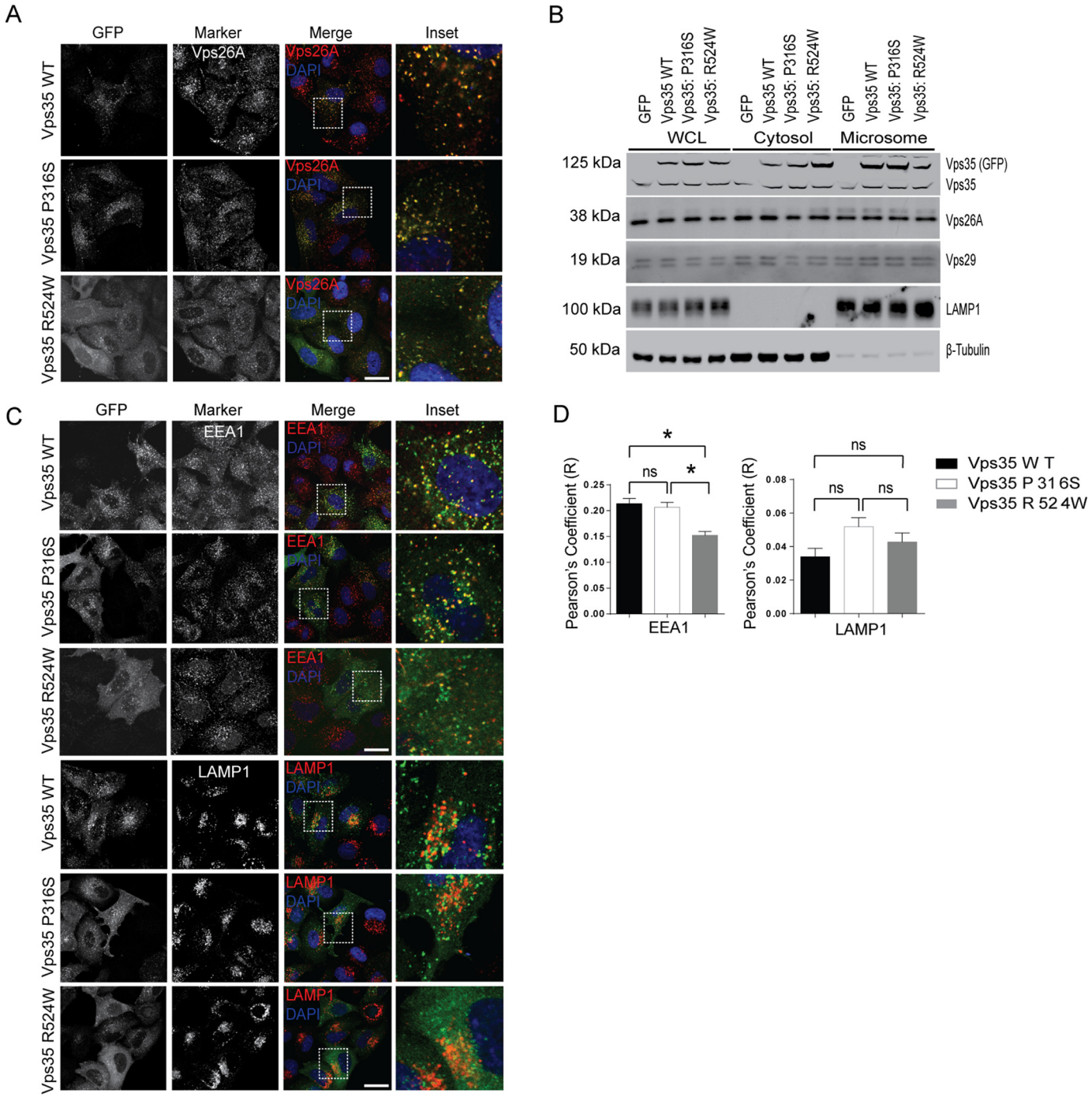

FIGURE 2. **Vps35 R524W disrupts recruitment of retromer to the endosomal membrane.** *A*, confocal analysis of HeLa cells transiently expressing Vps35 WT-GFP, Vps35 P316S-GFP, or Vps35 R524W-GFP immunolabeled with anti-Vps26A ($n = 3$, 10 images/group). *Scale bar*, 5 μm. *B*, representative immunoblotting ($n = 4$) of HeLa cells transiently expressing Vps35 WT-GFP, Vps35 P316S-GFP, or Vps35 R524W subjected to fractionation, SDS-PAGE, and immunolabeling with antibodies against the listed proteins. *C*, representative immunofluorescence images of HeLa cells transiently expressing Vps35 WT-GFP, Vps35 P316S-GFP, or Vps35 R524W-GFP labeled with EEA1 or LAMP1 followed by counterstaining with DAPI. *Scale bar*, 5 μm. *D*, analysis of co-localization from *c* represented by Pearson's correlation coefficient. Graphs representative of three independent experiments with 10 images/group with 5–7 transfected cells/field of view (*error bars*, S.E.; *, $p < 0.05$; *ns*, not significant; ANOVA with Tukey's multiple comparison test). *WCL*, whole cell lysate.

cargo sorting (25–27). We examined the subcellular localization of the WASH complex subunit FAM21, Rab7a, and TBC1D5 and their ability to interact with the retromer complex via co-immunoprecipitation following expression of Vps35 P316S-GFP and Vps35 R524W-GFP. HeLa cells transiently expressing GFP fusion constructs were fixed and immunolabeled with antibodies against endogenous FAM21 (Fig. 4*A*), Rab7a (Fig. 4*D*), and TBC1D5 (Fig. 4*G*). Consistent with previous findings, Vps35 WT-GFP or Vps35 P316S-GFP demonstrated a high level of co-localization ($R_{WT} = 0.8900$ and $R_{P316S} = 0.9035$; Fig. 4*B*) in contrast to cells expressing Vps35 R524W-GFP, where a significant decrease in co-localization with FAM21 ($R_{R524W} = 0.8011$; Fig. 4*B*) was observed. Similar to this, HeLa cells expressing Vps35 WT-GFP or Vps35 P316S-

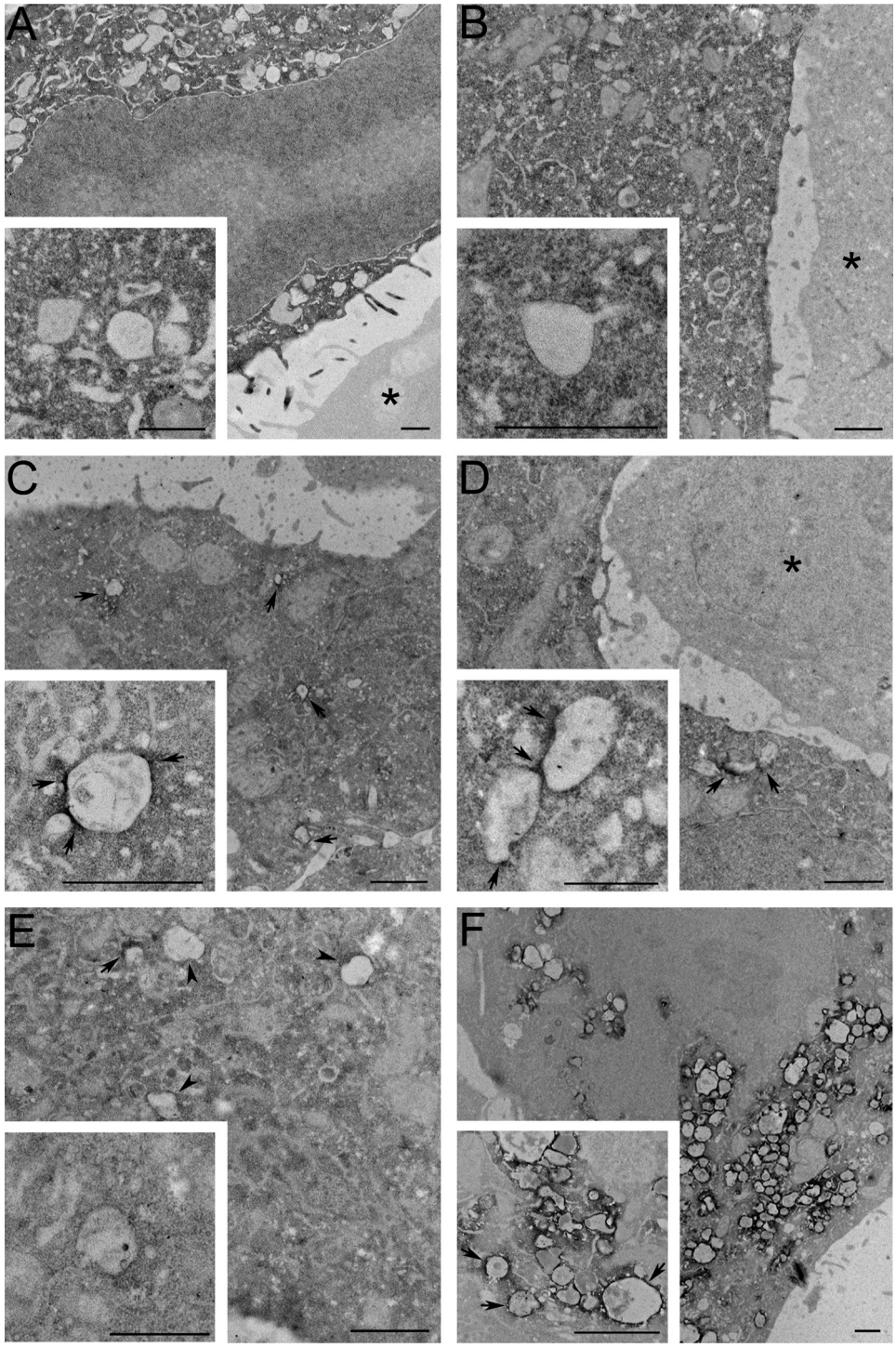

FIGURE 3. **Ultrastructural resolution of Vps35-GFP.** *A*, HeLa cells transfected with APEX-GBP alone demonstrate strong electron-dense reaction product in the cytoplasm. *B*, EGFP co-transfected with APEX-GBP results in exclusively cytoplasmic electron density. *C*, Vps35 WT-GFP + APEX-GBP demonstrates significant electron density at the endosomes of transfected cells. *Arrows*, endosomes with increased electron density compared with the cytoplasm. *D*, Vps35 P316S-GFP closely resembles the WT construct. *Arrows*, endosomes with increased electron density when compared with the cytoplasm. *E*, Vps35 R524W-GFP demonstrated a reduction in endosome association and an increase in soluble reaction product. *Arrows*, endosomes with enriched electron density over the cytoplasm; *arrowheads*, endosomes without electron density. *F*, Vps35 D620N-GFP caused enlarged endosomes with strong reaction product in transfected cells. *, untransfected adjacent cells. *Scale bars*, 1 μm.

GFP immunolabeled with antibodies against Rab7a or TBC1D5 displayed a moderate but consistent amount of co-localization (Rab7a, $R_{WT} = 0.2828$ and $R_{P316S} = 0.2856$; TBC1D5, $R_{WT} = 0.2967$ and $R_{P316S} = 0.2820$; Fig. 4, *E* and *H*, respectively). In contrast to these observations, expression of Vps35 R524W revealed a marked decrease in overlap with both Rab7a and TBC1D5 ($R_{R524W} = 0.2166$ and $R_{R524W} = 0.2056$; Fig. 4, *E* and *H*, respectively). Further, consistent with the previously described LAMP1 immunolabeling (Fig. 2*C*), Rab7a-positive endosomes demonstrated swelling following expression of

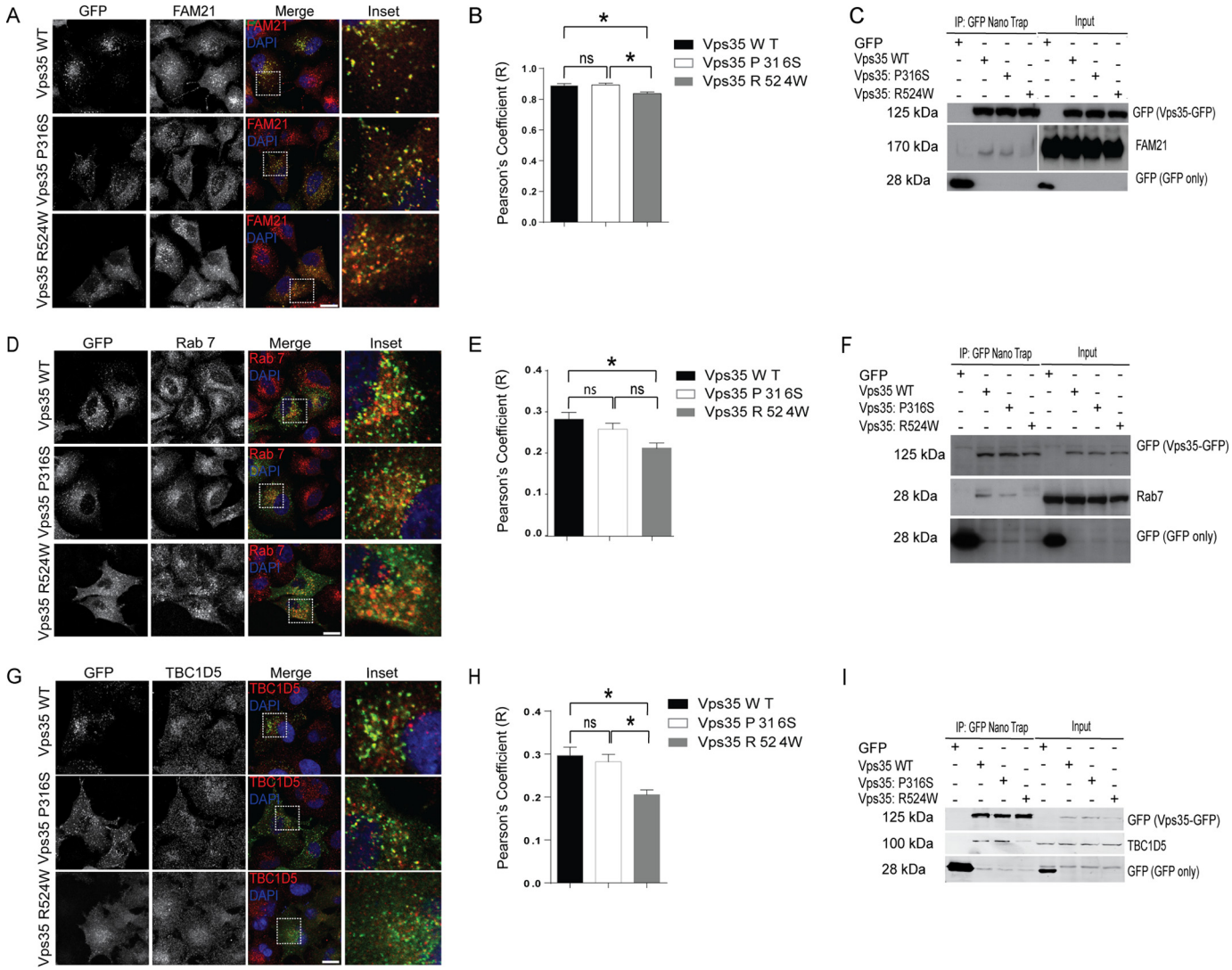

FIGURE 4. **Vps35 R524W has diminished association with regulators of retromer.** *A*, immunofluorescence staining of FAM21 in HeLa cells transiently expressing Vps35 WT-GFP, Vps35 P316S-GFP, and Vps35 R524W-GFP followed by DAPI counterstaining. *Scale bar*, 5 μm. *B*, analysis of co-localization from *A* represented by Pearson's coefficient. Graphs representative of three independent experiments with 10 images/group with 5–7 transfected cells/field of view (*error bars*, S.E.; *, $p < 0.05$; *ns*, not significant; ANOVA with Tukey's multiple comparison test). *C*, representative co-immunoprecipitation (*IP*) of GFP, Vps35 WT-GFP, Vps35 P316S-GFP, and Vps35 R524W-GFP with endogenous FAM21 from HeLa cells. *D*, representative immunofluorescence images of HeLa cells transiently expressing Vps35 WT-GFP, Vps35 P316S-GFP, or Vps35 R524W-GFP labeled with late endosome marker, Rab7. *Scale bar*, 5 μm. *E*, analysis of co-localization from *D* represented by Pearson's coefficient. Graphs are representative of three independent experiments with 10 images/group with 5–7 transfected cells/field of view (*error bars*, S.E.; *, $p < 0.05$; *ns*, not significant; ANOVA with Tukey's multiple comparison test). *F*, representative co-immunoprecipitation of GFP, Vps35 WT-GFP, Vps35 P316S-GFP, and Vps35 R524W-GFP with endogenous Rab7a from HeLa cells. *G*, localization of TBC1D5 in HeLa cells expressing Vps35 WT-GFP, Vps35 P316S-GFP, or Vps35 R524W-GFP counterstained with DAPI. *Scale bar*, 5 μm. *H*, analysis of co-localization from *G* represented by Pearson's coefficient. Graphs representative of three independent experiments with 10 images/group with 5–7 transfected cells/field of view (*error bars*, S.E.; *, $p < 0.05$; *ns*, not significant; ANOVA with Tukey's multiple comparison test). *I*, representative Western blots of TBC1D5 co-immunoprecipitation with Vps35 WT-GFP-, Vps35 P316S-GFP-, or Vps35 R524W-GFP-containing retromer from HeLa cells.

Vps35 R524W, but not Vps35 P316S or Vps35 WT, whereas endosomes positive for FAM21 or TBC1D5 displayed no evidence of gross morphological changes or differences in subcellular localization when compared with Vps35 WT-GFP or Vps35 P316S-GFP expression.

Co-immunoprecipitation was employed to investigate the ability of Vps35 P316S- and Vps35 R524W-containing retromer to interact with, FAM21, Rab7a, and TBC1D5 (Fig. 4). HeLa cells expressing GFP fusion constructs were lysed, and protein complexes were immunoprecipitated using GFP Nano-Trap, resolved by SDS-PAGE, and identified using Western blotting technique. Using antibodies against GFP and endogenous FAM21, Rab7a, and TBC1D5, no differences in the ability of Vps35 P316S-GFP-containing retromer to interact with FAM21, Rab7a, or TBC1D5 were observed, as determined by comparison with the levels of co-precipitated protein using Vps35 WT-GFP (Fig. 4, *C*, *F*, and *I*, respectively). In contrast, Vps35 R524W-GFP demonstrated a clear reduction in its capacity to co-precipitate FAM21, Rab7a, and TBC1D5, despite the total levels of all proteins being similar. Overall, Vps35 R524W consistently shows a decreased level of recruitment to endosomes, which is reflected in a lower level of interaction with proteins known to function in its recruitment to membranes. To determine whether the expression of Vps35 R524W

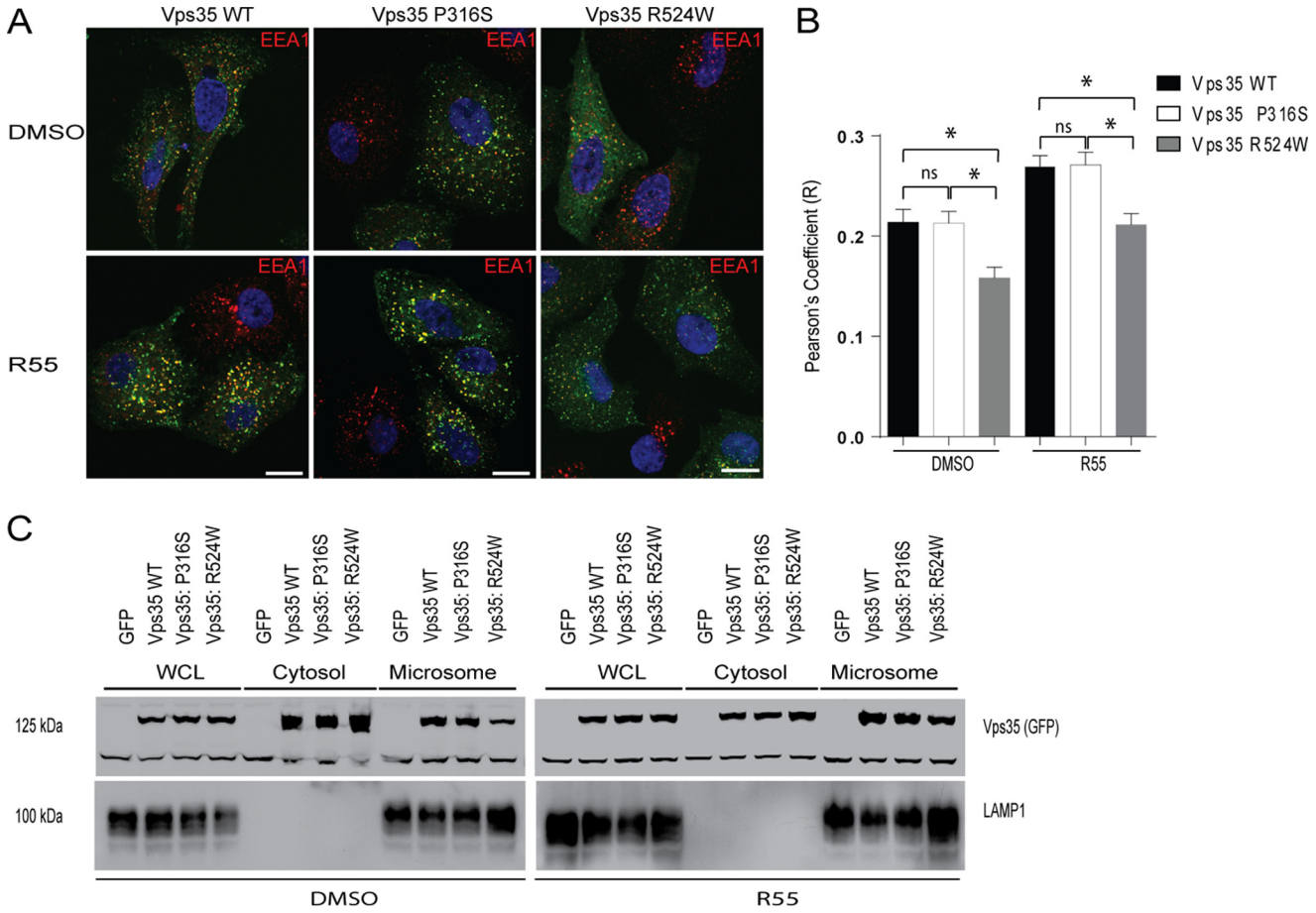

FIGURE 5. **Pharmacological stabilization of retromer increases its total levels and membrane recruitment.** *A*, confocal images of HeLa cells transiently expressing Vps35 WT-GFP, Vps35 P316S-GFP, or Vps35 R524W-GFP incubated with DMSO or 5 μM R55 immunolabeled with EEA1 and counterstained with DAPI. *Scale bar*, 5 μm. *B*, graphical representation of co-localization observed in *A* from two independent experiments with 10 images per construct and time point. *Error bars*, S.E.; *, $p < 0.05$; *ns*, not significant; ANOVA followed by Tukey's multiple comparison test. *C*, representative Western blots of HeLa cells transiently expressing GFP, Vps35 WT-GFP, Vps35 P316S-GFP, or Vps35 R524W-GFP treated with 5 μM R55 or DMSO for 48 h ($n = 3$). Membranes were also analyzed using anti-LAMP1 for a loading control.

was interfering with recruitment of these retromer-interacting proteins, we examined the level of co-localization between endogenous Vps26A and TBC1D5. A non-significant change was observed between control cells and those expressing the Vps35-GFP proteins (data not shown), consistent with these PD-associated Vps35 variants not interfering with endogenous retromer recruitment.

Vps35 R524W Expression Induces α-Synuclein Aggregation—Next, we employed the recently described retromer-stabilizing agent (28) R55 in an attempt to rescue the diminished membrane recruitment of Vps35 R524W-GFP-containing retromer. For this, we employed both immunofluorescence and biochemical methodologies described above. HeLa cells transiently expressing Vps35 WT-GFP, Vps35 P316S-GFP, or Vps35 R524W-GFP were incubated with 5 μM R55 or DMSO control for 48 h, fixed, and immunolabeled with the early endosomal marker, EEA1. As previously observed (Fig. 2*C*), in cells incubated with DMSO vehicle control, co-localization analysis between GFP and EEA1 showed a decrease in Vps35 R524W-GFP at the early endosome ($R_{WT} = 0.214$, $R_{P316S} = 0.213$, and $R_{R524W} = 0.158$; Fig. 5, *A* and *B*). Interestingly, treatment of cells transfected with Vps35 R524W-GFP and treated with R55 agent demonstrated an increased endosomal localization (Fig. 5, *A* and *B*, $R_{WT} = 0.269$, $R_{P316S} = 0.271$, and $R_{R524W} = 0.211$). In agreement with this observation, biochemical fractionation of cells transfected with GFP, Vps35 WT-GFP, Vps35 P316S-GFP, or Vps35 R524W-GFP showed an increase in the total level of Vps35 WT-GFP and Vps35 P316S-GFP and a marked shift of Vps35 R524W-GFP from the cytosolic to microsome fraction (Fig. 5*C*). However, the presence of R55 did not completely rescue the loss of Vps35 R524W-GFP in the microsome fraction to a level equivalent to that observed for Vps35 WT-GFP or Vps35 P316S-GFP (Fig. 5*C*).

α-Synuclein is the major component of LBs, a prominent phenotype in PD pathogenesis. Although the underlying cause of LB formation is not fully understood, it appears to be caused by the perturbation of several distinct cellular homeostasis processes, including defects in endosomal degradation pathways (29, 30). To address whether retromer plays a role in the accumulation of aggregated α-synuclein, we used the SH-SY5Y neuroblastoma cell model, which endogenously expresses α-synuclein, possesses machinery needed for dopamine uptake and metabolism, and responds to external stimuli, including depolarization using KCl (31). To confirm the suitability of this assay, the induced α-synuclein aggregates were confirmed to contain phosphorylated α-synuclein (32), autophagy compo-

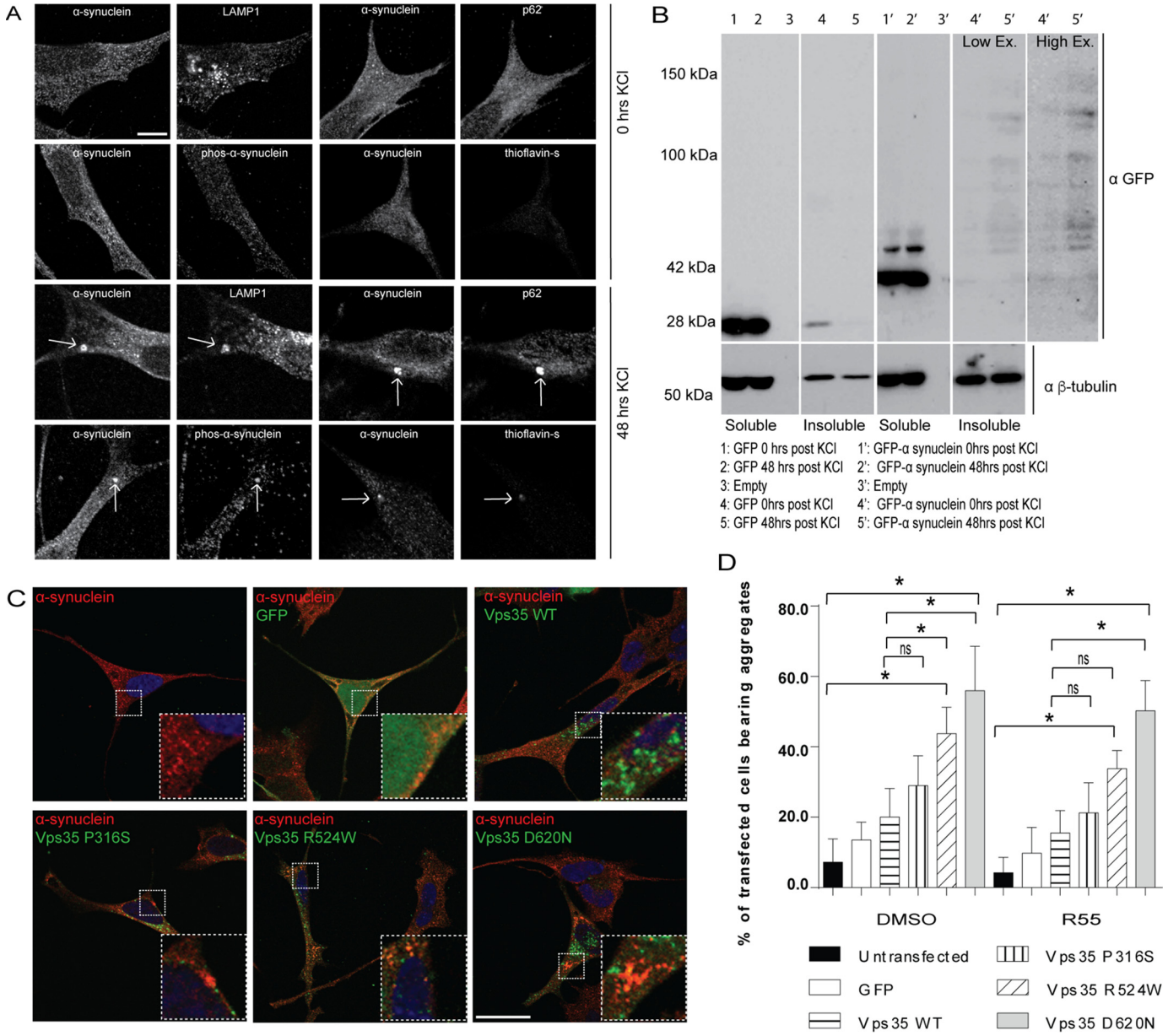

FIGURE 6. **Parkinson disease-linked Vps35 point mutations increase the production of α-synuclein-positive aggregates.** *A*, SH-SY5Y cells were untreated or were induced by KCl treatment to form α-synuclein aggregates (*arrows*), and immunofluorescence was performed with anti-α-synuclein in combination with antibodies to phosphorylated α-synuclein (phospho-Ser-129), autophagy marker p62, lysosome marker LAMP1, and protein aggregation marker thioflavin-S. *Scale bar*, 2 μm. *B*, SH-SY5Y cells stably expressing GFP alone or GFP-α-synuclein were depolarized with 50 mM KCl for 60 min or sham-treated and left to recover for 48 h. Soluble and insoluble fractions were generated and analyzed by Western blotting as described under "Experimental Procedures." 40 μg of protein was loaded in each lane. A higher exposure (*High Ex.*) of the GFP-α-synuclein is shown, whereas the lower exposure (*Low Ex.*) is equivalent to the soluble fraction. *C*, confocal immunofluorescence images of SH-SY5Y cells expressing GFP fusion constructs, immunolabeled with anti-α-synuclein, and counterstained with DAPI following treatment with KCl. *Scale bar*, 5 μm. *D*, graph representing the number of transfected SH-SY5Y cells bearing α-synuclein aggregates following KCl treatment before incubation with DMSO or 5 μM R55 for 48 h. The graph represents the proportion of cells with α-synuclein aggregated from 20–30 random images from three independent experiments. *Error bars*, S.E.; *, $p < 0.05$; *ns*, not significant; ANOVA followed by Tukey's multiple comparison test.

nent p62 (32, 33), and lysosome marker, LAMP1 (34) (Fig. 6*A*). These aggregates are also thioflavin-S-positive, indicating that some of the aggregated α-synuclein is in a fibrillary form (Fig. 6*A*). Furthermore, the ability of this method to induce higher molecular weight aggregates of GFP-α-synuclein was confirmed biochemically (Fig. 6*B*). All of these properties have been associated with α-synuclein aggregates formed in other Parkinson disease models and/or Lewy bodies.

The reduced recruitment of Vps35 R524W to endosomes would impair the retromer's function; therefore, the expression of this Vps35 PD-associated mutant may reduce α-synuclein clearance and promote aggregation. Untransfected SH-SY5Y cells and cells expressing GFP, Vps35 WT-GFP, Vps35 D620N-GFP, Vps35 P316S-GFP, or Vps35 R524W-GFP were incubated with 50 mM KCl for 60 min and allowed to recover in complete growth medium for 48 h and immunolabeled for endogenous α-synuclein, and transfected cells were scored as positive or negative for aggregates. α-Synuclein-positive aggregates were observed in 7.2% of untransfected SH-SY5Y cells, 13% of SH-SY5Y cells expressing GFP, and 20% of those expressing

Vps35 WT-GFP. In comparison with these control cells, 29% of Vps35 P316S-GFP-expressing cells, 43% of Vps35 R524W-GFP-expressing cells, and 56% of Vps35 D620N-GFP-expressing cells were observed to have α-synuclein aggregates (Fig. 6, *C* and *D*). Concurrent treatment of untransfected SH-SY5Y cells with 5 μM R55 for 48 h resulted in a consistent reduction in the total percentage of aggregates observed (4%) (Fig. 6*D*). Likewise, a reduction in the total number of aggregates was witnessed in R55-treated SH-SH5Y cells expressing GFP or Vps35 WT-GFP (9 and 15%, respectively). This trend was also observed for SH-SY5Y cells expressing either Vps35 P316S-GFP (21%) or Vps35 R524W-GFP (33%); however, this was not seen in cells expressing Vps35 D620N-GFP (50.2%; Fig. 6*D*), potentially due to its nature as a likely dominant negative protein. Therefore, the expression of these PD-associated Vps35 mutants can directly influence the formation of large α-synuclein-positive aggregates, a hallmark of PD.

Retrograde Sorting Is Delayed in the Presence of Vps35 R524W—To test the functional impact of Vps35 R524W expression on the retrograde endosomal cargo sorting, we investigated the recycling of the well characterized retromer cargo, CI-M6PR. Previous reports mapped the interaction between retromer and the cytosolic tail of the CI-M6PR to amino acids 500–693 of the Vps35 subunit (11). Given the location of the point mutations on the Vps35 in relation to the Vps29 and the cargo-interacting domain within Vps35, the interaction of retromer with CI-M6PR, modulation of soluble lysosomal enzyme delivery, relative co-localization, and kinetics of retrograde trafficking were analyzed as described previously (10, 11, 17). Vps35 P316S-containing retromer was found to co-precipitate the M6PR at levels identical to that of the wild-type retromer, whereas Vps35 R524W displayed decreased levels of M6PR (ranging from 15 to 60% less precipitant than Vps35 WT levels) (Fig. 7*A*). Expression of Vps35 P316S-GFP, like Vps35 WT-GFP, did not disrupt the lysosomal delivery of cathepsin D, which is dependent on mannosylation and binding to the CI-M6PR for the transport of the Golgi-processed precursor into the endosomal system. In contrast, expression of Vps35 R524W-GFP clearly disrupted the trafficking itinerary of the CI-M6PR because secretion of pro-cathepsin D into the extracellular medium was observed after protein synthesis was inhibited for 7 h (Fig. 7*B*). Next, the subcellular distribution of the endogenous CI-M6PR relative to retromer was examined. The CI-M6PR was localized to punctate and perinuclear organelles in cells transfected with Vps35 WT-GFP and Vps35 P316S-GFP and demonstrated a small amount of overlap with retromer ($R_{WT} = 0.210$ and $R_{P316S} = 0.204$; Fig. 7, *C* and *D*). In comparison, expression of Vps35 R524W-GFP was found to alter the subcellular distribution of the CI-M6PR from predominantly perinuclear staining to dispersed puncta. These dispersed CI-M6PR-positive puncta demonstrated increased co-localization with the Vps35 R524W-GFP endosomal retromer ($R_{R524W} = 0.261$) relative to controls. Given the observed deficit in retrograde trafficking, we investigated the Golgi morphology in HeLa cells transfected with all GFP constructs using antibodies against *trans*-Golgi protein, p230. HeLa cells expressing the described constructs demonstrated no marked differences in overall Golgi morphology or distribution (data not shown).

HeLa cells were co-transfected with CD8-CI-M6PR to monitor the retrograde delivery of internalized antibodies to the TGN using a well established antibody uptake assay (10). Cells were incubated on ice with anti-CD8 antibody and chased at 37 °C for up to 30 min. In cells expressing CD8-CIM6PR and GFP only, strong CD8 immunostaining was observed on membranes positive for p230, demonstrating efficient delivery of the reporter to the TGN network following retromer-mediated transport through the endosome. Consistent with this, strong CD8 immunostaining was observed to overlap with p230-positive membranes in cells expressing either Vps35 WT-GFP or Vps35 P316S-GFP at 30 min post-chase (Fig. 7*E*). However, in cells expressing Vps35 R524W-GFP, the majority of the p230-positive membranes did not display evidence of CD8 staining at 30 min post-chase and showed strong CD8-CIM6PR localization to dispersed punctate structures, reminiscent of endosomes, indicative of significant delays in the retrograde sorting pathway (Fig. 7*E*). Based on these multiple assays, the expression of the PD-associated Vps35 R524W mutant retromer protein significantly impacts the retrograde trafficking pathway and accumulates CI-M6PR in endosomes due to an inefficiency in transporting proteins from endosomes to the TGN.

SNX27 (Sorting Nexin 27)-Retromer-dependent Recycling of GLUT1 Is Unaffected in the Presence of Vps35 R524W—In addition to retrograde trafficking of cargo, retromer also functions to recycle proteins from endosomes to the plasma membrane by forming a complex with SNX27 (35, 36). To determine whether Vps35 P316S-GFP or Vps35 R524W-GFP expression impacts the retromer-mediated recycling pathway, we investigated the subcellular localization of endogenous SNX27 in transfected HeLa cells (Fig. 8, *A* and *B*). Co-localization analysis revealed a moderate overlap between both Vps35 WT-GFP and SNX27 ($r = 0.3562$) and Vps35 P316S-GFP with SNX27 ($r = 0.3851$), whereas analysis of Vps35 R524W-GFP with SNX27 demonstrated a marked reduction in co-localization ($r = 0.2659$; Fig. 8*B*). Membrane fractionation showed unchanged levels of SNX27 recruited to membranes (data not shown), and the subcellular localization relative to endogenous Vps26A (Fig. 8*C*) and overall, the SNX27-positive endosome morphology in the presence of Vps35 R524W-GFP was unaltered (Fig. 8*A*), consistent with the notion that SNX27 is recruited to the endosome independent of the retromer complex. Relative to Vps35 WT-GFP, less SNX27 was co-immunoprecipitated with Vps35 R524W-GFP (Fig. 8*D*). To determine whether this decrease in SNX27 binding to Vps35 R524W retromer had a dominant negative effect on the recycling pathway as it does for the retrograde pathway, we analyzed GLUT1 as a representative and well established SNX27-retromer-dependent cargo (36, 37). HeLa cells expressing Vps35 WT-GFP, Vps35 P316S-GFP, or Vps35 R524W-GFP were immunolabeled with antibodies raised against endogenous GLUT1 and LAMP1 (Fig. 8*E*). Confocal microscopy revealed localization of GLUT1 to both the cell surface and punctate structures in cells expressing Vps35 WT-GFP, Vps35 P316S-GFP, or Vps35 R524W-GFP, reminiscent of the neighboring untransfected cell staining. Additionally, intracellular localization of GLUT1 demon-

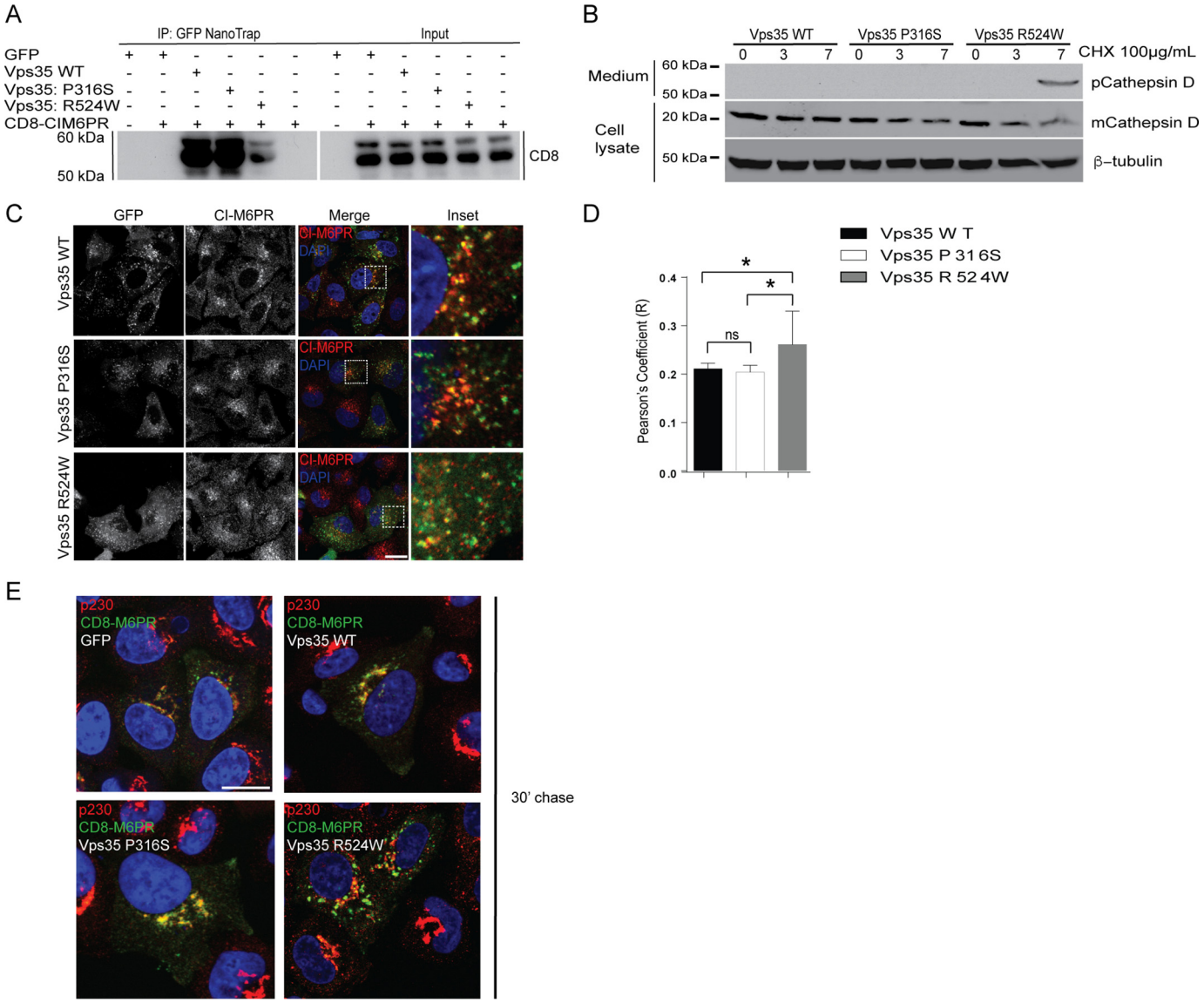

FIGURE 7. **Expression of Vps35 R524W perturbs localization and sorting of CI-M6PR.** *A*, representative co-immunoprecipitation of GFP fusion constructs with CD8-M6PR reporter resolved by SDS-PAGE. Membranes were immunolabeled with anti-CD8. *B*, representative immunoblots of culture medium and cell lysates from HeLa cells transiently transfected with Vps35 WT-GFP, Vps35 P316S-GFP, or Vps35 R524W-GFP and incubated with 100 μg/ml cyclohexamide for up to 7 h ($n = 3$). Membranes were probed with antibodies raised against β-tubulin and cathepsin D. *C*, confocal analysis of HeLa cells transiently expressing Vps35 WT-GFP, Vps35 P316S-GFP, or Vps35 R524W immunolabeled with antibodies against endogenous CI-M6PR and counterstained with DAPI. *Scale bar*, 5 μm. *D*, graphical representation of co-localization observed in *C*. The graph represents three independent experiments with 10 images/group with 5–7 transfected cells/field of view ($n = 3$; *error bars*, S.E.; *, $p < 0.05$; *ns*, not significant; ANOVA followed by Tukey's multiple comparison test). *E*, representative images of HeLa cells expressing CD8-CIM6PR and GFP fusion constructs at 30 min post-chase with anti-CD8 and immunolabeled with anti-p230 (*red*) and anti-CD8 (*green*) antibodies. *Scale bar*, 5 μm.

strated minimal overlap with late endosome marker, LAMP1, supporting uninterrupted recycling in the presence of Vps35 P316S-GFP or Vps35 R524W-GFP (Fig. 8*E*). To further confirm these results, we labeled the plasma membrane of transfected cells with biotin and used streptavidin-based precipitation to assess the cell surface levels of GLUT1 and TfnR. Biotinylation revealed similar cell surface levels of retromer-dependent cargo, GLUT1, and retromer-independent receptor, TfnR, in cells expressing GFP, Vps35 WT-GFP, Vps35 P316S-GFP, or Vps35 R524W-GFP. We also found that Vps35 D620N expression did not impact recycling of GLUT1 (Fig. 8*F*), consistent with previous reports (19). In support of this finding, HeLa cells expressing all GFP fusion constructs demonstrated identical levels of glucose uptake compared with controls, which was consistent with GLUT1 biotinylation observations (Fig. 8*G*). Therefore, the reduced levels of Vps35 R524W-GFP from SNX27-positive endosomes do not appear to negatively impact the recycling function of retromer.

Discussion

Although the PD-linked point mutation Vps35 P316S does not destabilize the retromer's high affinity trimer structure, Vps35 R524W displayed some evidence of impaired trimer formation, modulation of retromer's cellular functions, and induction of α-synuclein aggregation, which is an underlying hallmark of PD. Despite genetic evidence linking this mutation to

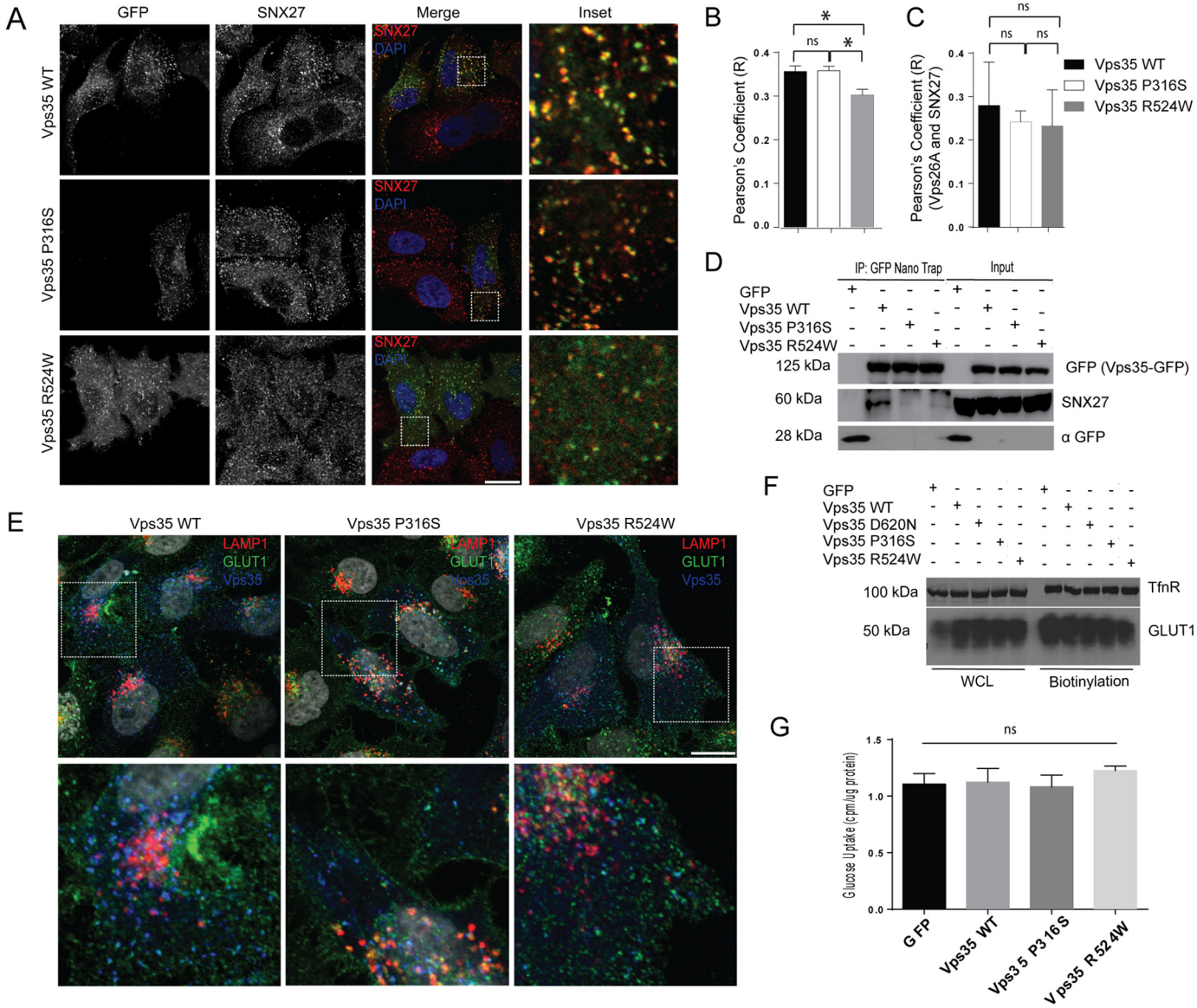

FIGURE 8. **Vps35 R524W does not disrupt SNX27-dependent cargo recycling.** *A*, immunofluorescence of HeLa cells transiently expressing Vps35 WT-GFP, Vps35 P316S-GFP, or Vps35 R524W-GFP immunolabeled with anti-SNX27. *Scale bar*, 5 μm. *B*, graphical representation of co-localization observed in *A*. Graphs are representative of three independent experiments with 10 images/group with 5–7 transfected cells/field of view (*error bars*, S.E.; *, $p < 0.05$; *ns*, not significant; ANOVA followed by Tukey's multiple comparison test). *C*, Pearson's coefficient of SNX27 with Vps26A in HeLa cells expressing Vps35 WT-GFP, Vps35 P316S, or Vps35 R524W-GFP (*error bars*, S.E.; *, $p < 0.05$; *ns*, not significant; ANOVA followed by Tukey's multiple comparison test). *D*, co-immunoprecipitation (*IP*) using GFP NanoTrap of GFP, Vps35 WT-GFP, Vps35 P316S-GFP, and Vps35 R524W-GFP with endogenous SNX27. *E*, representative immunofluorescence images of HeLa cells expressing Vps35 WT-GFP, Vps35 P316S-GFP, or Vps35 R524W-GFP followed by co-immunolabeling with anti-GLUT1 and anti-LAMP1. *Scale bar*, 5 μm. *F*, representative Western blots ($n = 3$) of HeLa cells expressing GFP fusion constructs showing biotinylation of cell surface and total GLUT1 levels. *G*, graphical demonstration of glucose uptake in HeLa cells transiently transfected with GFP fusion constructs. *ns*, not significant. Data are representative of three independent experiments conducted in triplicate. *Error bars*, S.E.

late onset PD, expression of Vps35 P316S did not display any distinct cellular phenotypes when compared with expression of Vps35 WT. Vps35 R524W demonstrated poor recruitment to the endosome, and its incorporation negatively impacted the interaction of retromer with several well established retromer-interacting proteins. Further, this mislocalization of Vps35 R524W-containing retromer resulted in reduced endosome-to-Golgi but not endosome-to-plasma membrane receptor sorting. This was demonstrated by several CI-M6PR trafficking assays, where we show the redistribution of endogenous CI-M6PR from the perinuclear space to dispersed puncta, late endosome swelling, and detectable levels of pre-cathepsin D in the culture medium, which were mirrored by the decrease in cathepsin D processing in the cells. Finally, we demonstrate that expression of the R524W mutation leads to increased levels of α-synuclein-positive aggregation.

Previous studies demonstrate the recruitment of additional endosomal machinery, such as the WASH complex, TBC1D5, and members of the SNX-BAR, to the endosome assist retromer in mediating sorting of its cargo to the TGN (20, 38, 39). However, it is the combination of the small GTPase Rab7a and phox homology (PX)-containing protein SNX3 that is thought to initiate this cascade by recruiting retromer to the membrane (24, 40). The current view of retromer mediated transport is

that the Vps35-Vps26-Vps29 proteins form a stable core trimer that is a hub for associating with regulatory and cargo proteins (25). Our data show that although the core complex remains unaffected by the P316S, the R524W mutation partially disrupts this formation and also negatively impacts the association with regulatory molecules needed for cargo sorting. Previously, Vps35-Rab7a-SNX3 interaction studies demonstrated that binding of Rab7a and SNX3 is within the first 300 amino acids of Vps35 and immediately adjacent to the Vps26-Vps35 interface (41). Despite this, we showed that R524W, but not the P316S mutation within Vps35, severely impacts the retromer-Rab7a interaction and Vps35 R524W-retromer membrane association, coupled with reduced interactions with the WASH complex subunit FAM21, the RabGAP TBC1D5, and PDZ motif cargo adaptor SNX27. Whereas Vps35 R524W-retromer displayed impaired binding to multiple retromer-associated proteins, we suggest that this is a consequence of reduced endosome recruitment rather than a direct impact on the binding surfaces of all of these molecules. Interestingly, the use of R55, a recently described retromer-stabilizing agent (28), showed a rescue phenotype in membrane association of the Vps35 R524W-retromer, possibly by stabilizing a conformational change needed for retromer-Rab7a interaction required for membrane recruitment. Therefore, these findings suggest that the observed defect in Vps35 R524W-expressing cells arises from its diminished interaction with machinery needed to recruit retromer to the membrane, second to a partial loss of stable incorporation into the retromer trimer.

Given the described role of CI-M6PR in trafficking of cathepsin D, a protease needed for clearance of α-synuclein (42, 43), and the importance of retromer in correct localization of the CI-M6PR and sorting of lysosomal cathepsin D (11, 13, 44), it is not unexpected that expression of Vps35 mutants that perturb trafficking demonstrates increased frequency of forming intracellular aggregates. Additionally, a complete knock-out of cathepsin D leads to extensive levels of high molecular weight α-synuclein species and an increase in Lewy Body numbers in brains of knock-out animals (30). Together, these findings support the concept that regulation of the lysosomal pathway and its lumenal content plays a fundamental role in turnover of proteins, a pathway that is already highly susceptible to errors during aging (45). To examine the role of retromer in α-synuclein aggregation and clearance, we used a non-pharmacological based stimulus (KCl) rather than other reagents (Rotenone, Bafilomycin A1) that target mitochondrial and lysosomal function, respectively, and may indirectly impact the retromer's cellular function (46, 47). Using this assay, our findings indicate that the expression of Vps35 R524W leads to CI-M6PR and cathepsin D mistrafficking, suggesting a direct correlation between the loss of retromer, the Vps35 R524W point mutation, and the production of α-synuclein aggregates in a cellular system. Consistent with these results, the previously described PD-linked Vps35 mutation (Vps35 D620N) was also reported to impair the degradation of α-synuclein, a product of diminished endolysosomal functionality, further supporting a relationship between receptor trafficking and α-synuclein aggregate production (21). Several lines of evidence also demonstrate the requirement of both Rab7 and TBC1D5 in maintaining constant autophagic flux, retromer-dependent trafficking, and optimal function of the lysosomal compartment (30, 38, 48–50). Although these studies do not conclusively demonstrate a direct link between the retromer complex, autophagic flux itself, and formation of α-synuclein aggregates, they do support the emerging notion that retromer-dependent machinery is required for functionality of the endolysosomal-autophagy clearance pathways.

The interaction between the SNX27 PDZ domain and the Vps26 subunit of the retromer complex has been shown to be important in regulation of the recycling pathway (37), but their recruitment to the endosomal membrane appears to be independent of each other (36). Here we confirm that the membrane association of SNX27 is not impaired in the presence of Vps35 R524W expression and also demonstrate that recycling of GLUT1, a known PDZ motif-containing cargo, was identical to that observed in the presence of Vps35 WT-GFP expression. This may be due to the interaction of the endogenous SNX27 with the more abundant, endogenous retromer over the poorly recruited Vps35 R524W-retromer leading to the uninterrupted recycling of SNX27-dependent cargo observed here. Therefore, the PD-linked R524W mutation does not influence the recycling trafficking pathway in our experimental conditions, like the PD-linked Vps35 D620N mutation, which appears to be similarly functional in GLUT1 recycling.

Overall, we have demonstrated that Vps35 R524W-containing retromer poorly interacts with known endosomal machinery and consequently impacts the retrograde cargo sorting properties of the retromer complex and not its role in recycling SNX27-dependent cargo. Expression of Vps35 R524W is similar to the sorting defect witnessed for the Vps35 D620N mutation linked to PD, in which the CI-M6PR is not efficiently delivered to the TGN (7, 17, 19). However, Vps35 D620N-containing retromer reportedly interacts with accessory proteins TBC1D5 and SNX27, to the same degree as wild-type retromer, but has minor reductions in its ability to interact with the WASH complex (19, 21), whereas Vps35 R524W has reduced interactions with TBC1D5, SNX27, and the WASH complex. Vps35 D620N broadly modifies endosome morphology (17), whereas Vps35 R524W expression alters late endosome morphology with minimal enrichment at the endosome, supporting very distinct changes to the molecular and cellular properties of the retromer sorting pathways in the presence of the two mutations. Despite these described differences between the D620N and R524W Vps35 PD-linked mutations, it is clear that the retrograde sorting properties of retromer, and not its role in endosome to plasma membrane trafficking, are indeed defective in PD. Although this does not rule out Vps35 P316S as being causative in PD, it implies that the primary defect leading to disease onset may be through a currently undefined retromer-dependent mechanism.

Experimental Procedures

DNA Constructs—Vps35 WT-GFP has been described previously (17) and was used to generate P316S and R524W point mutations. QuikChange mutagenesis (Stratagene) was employed using the following PCR mutagenic primer pairs: 5′-GCTCACCGTGAAGATGGATCCGGAATCCCAGCG-

GAT and 3′-ATCCGCTGGGATTCCAGGACCATCTTCACGGTGAGC or 5′-GCTGGTGGAAATCAGTGGATTCGCTTCACACTG and 3′-CAGTGTGAAGCGAATCCACTGATTTCCACCAGC, respectively. The pCMU-CD8/CI-M6PR and Vps35 D620N-GFP constructs were described previously (17).

Antibodies—The following primary antibodies were purchased as indicated: mouse monoclonal anti-CIM6PR, anti-α-synuclein, anti-SNX27 (C16), rabbit polyclonal anti-GLUT1, anti-SQSTM1/p62, anti-Vps26A, and rabbit monoclonal anti-α-synuclein (phospho-Ser-129) (Abcam); mouse monoclonal anti-GFP and rabbit polyclonal anti-GFP (Life Technologies, Inc., and Roche Applied Science, respectively); goat polyclonal raised against Vps35 (IMGENEX); mouse monoclonal anti-human EEA1, p230, and LAMP1 (BD Transduction Laboratories); rabbit monoclonal anti-Rab7a (Cell Signaling); mouse monoclonal anti-CD8 (eBioscience); mouse monoclonal anti-β-tubulin (Sigma-Aldrich); sheep polyclonal anti-TGN-46 (AbD Serotec); goat polyclonal anti-TBC1D5 (C-14) (Santa Cruz Biotechnology); and rabbit polyclonal anti-cathepsin D and anti-FAM21C (Merck Millipore). Rabbit polyclonal against Vps29 was generated in house and used previously (10). Secondary goat anti-mouse IgG Alexa Fluor 568, donkey anti-mouse IgG Alexa Fluor 546, and donkey anti-goat IgG Alexa Fluor 647 were from Life Technologies; horseradish peroxidase-conjugated anti-rabbit and anti-mouse antibodies were from Dako; and IRdye 680- and IRdye 800-conjugated fluorescence secondary antibodies were from LI-COR Biosciences.

Cell Culture and Transfection—HeLa cells were grown in a humidified 37 °C incubator with 5% CO_2 and maintained in DMEM supplemented with 10% FBS (Gibco) and 2 mM L-glutamine (Life Technologies). SH-SY5Y cells (Sigma-Aldrich) were maintained in Roswell Park Memorial Institute (RPMI) medium supplemented with 10% FBS (Gibco) and 2 mM L-glutamine (Life Technologies). Mammalian constructs were transfected into cells using Lipofectamine 2000 (Life Technologies) according to the manufacturer's instructions. This routinely achieved 50–70% transfection efficiency for HeLa cells and 25–40% for SH-SY5Y cells.

Protein Purification and ITC—Constructs of mouse VPS35, VPS29, and VPS26A for expression in *Escherichia coli* were described previously (17), and all VPS35 point mutations were engineered using the QuikChange mutagenesis kit (Stratagene). Recombinant proteins used for the ITC experiments were prepared and analyzed as described (51). Experiments were performed in 20 mM Tris (pH 8.0), 200 mM NaCl, 1 mM DTT at 283 K using a MicroCal iTC200 (GE Healthcare).

Immunoprecipitations—Transfected HeLa cell monolayers were washed in ice-cold PBS and lysed in TK lysis buffer (50 mM HEPES, 150 mM NaCl, 1% Triton X-100, 10 mM $Na_4P_2O_7$, 30 mM NaF, 2 mM Na_3VO_4, 10 mM EDTA, 0.5 mM AEBSF, and Complete Mini protease inhibitor mixture (Roche Applied Science)) for 10 min on ice. Whole cell lysates were centrifuged at 17,000 × *g*, and supernatant was collected. These supernatants were incubated with GFP-NanoTrap beads for 1–2 h or anti-Vps26A antibodies overnight at 4 °C under constant rotation. Vps26A antibodies were complexed by the addition of Protein G-Sepharose beads. GFP immunoprecipitation performed from isolated cytosol was conducted in HES buffer described below. Complexes were dissociated from the beads by boiling after three consecutive washes with TK lysis buffer.

Western Immunoblotting—Cell lysate samples were subjected to a bicinchoninic acid (BCA) assay (Thermo Scientific) to determine protein concentration. Equivalent amounts of protein per sample (10–50 μg) were resolved by SDS-PAGE and transferred onto PVDF membrane (Immobilon-P and Immobilon-FL, Millipore) according to the manufacturer's instructions. Immunoblotting using ECL and the Odyssey infrared imaging system (LI-COR) was performed as per the manufacturer's instructions.

Electron Microscopy—EM was performed as described previously (23). Briefly, HeLa cells were seeded onto 3-cm dishes and transfected with a DNA ratio of 1:1 GFP-tagged protein of interest to APEX-GBP using Lipofectamine 2000 (Invitrogen) as per the manufacturer's instructions. Cells were fixed in 2.5% glutaraldehyde in 0.1 M sodium cacodylate buffer for 1 h at room temperature and washed repeatedly in 0.1 M sodium cacodylate buffer. The diaminobenzoic acid reaction was performed for 30 min at room temperature in the presence of H_2O_2. Cells were then post-fixed in 1% osmium tetroxide for 2 min and then washed again in 0.1 M sodium cacodylate. Cells were serially dehydrated in increasing percentages of ethanol and subsequently serially infiltrated with increasing percentages of LX112 resin and polymerized at 60 °C overnight. Ultrathin sections (60 nm) were cut on an Ultracut UC6 ultramicrotome (Leica) and on a JEOL 1011 electron microscope at 80 kV fitted with a Morada Soft Imaging camera (Olympus) at 2-fold binning.

Indirect Immunofluorescence, Confocal Microscopy, and Colocalization Analysis—HeLa cells grown on glass coverslips were washed with room temperature PBS twice before fixation with 4% paraformaldehyde for 20 min. Cells were permeabilized using 0.1% Triton X-100/PBS for 10 min at room temperature and subsequently blocked using 2% BSA/PBS for 45 min. Cells were labeled with primary and secondary antibodies and counterstained with DAPI nuclear stain. Coverslips were mounted using fluorescent mounting medium (Dako) and imaged using a Zeiss LSM710 upright scanning laser confocal fluorescent microscope equipped with a ×63 plan-apochromatic objective and argon, HeNe1, HeNe3 lasers.

All images were analyzed using Zeiss LSM version 5.0 and Adobe Photoshop software. Pearson's correlation coefficients were calculated using the ImageJ plugin "Colocalization finder" (National Institutes of Health). Fields of view containing both transfected and non-transfected cells were segregated by generating regions of interest around transfected cells, cropping selected regions, splitting into respective grayscale channels, and applying threshold settings. Co-localization analysis was conducted on three independent experiments with 10 images/group containing 5–10 transfected cells/field of view. Co-localization values were exported to GraphPad Prism version 5 software and tabulated accordingly.

Microsomal Fractionation—HeLa cells grown in 15-cm^2 culture dishes were washed twice on ice in PBS, collected, and homogenized with 20 passages through a 22-gauge ¾ needle in buffer containing 20 mM HEPES, pH 7.4, 250 mM sucrose, 1 mM

EDTA, 2 mM Na_3VO_4, 10 mM EDTA, and 0.5 mM AEBSF. Lysates were spun at 500 × *g* for 5 min, and a portion of the resulting supernatant was collected and stored as the whole cell lysate. The resulting supernatant was further centrifuged at 17,200 × *g* for 20 min to isolate the crude plasma membrane fraction followed by 175,000 × *g* for 75 min to isolate the microsome fraction from the remaining cytosolic fraction. Pelleted microsomes were resuspended in homogenization buffer (20 mM HEPES, pH 7.4, 250 mM sucrose, 1 mM EDTA, 2 mM Na_3VO_4, 10 mM EDTA, and 0.5 mM AEBSF).

α-Synuclein Aggregation—SH-SY5Y cells grown on glass coverslips were incubated with 50 mM KCl (Sigma-Aldrich) for 60 min at 37 °C. Following the treatment, cells were either fixed (0 h time point) or allowed to recover in complete growth medium for up to 48 h, when they were fixed and immunofluorescence microscopy was performed using anti-α-synuclein antibody. For detection of α-synuclein aggregates by Western blotting, SH-SY5Y cells stably expressing GFP-α-synuclein (52) were collected for analysis 48 h after KCl treatment as described (53) and resolved on a 6% SDS-PAGE to separate high molecular weight α-synuclein. Thioflavin-S (Sigma-Aldrich) staining was employed following washes with ethanol and performed as described (54).

Cathepsin D Secretion Assay—HeLa cells plated in 6-well dishes 48 h before use were washed in 37 °C PBS and incubated with serum-free DMEM supplemented with 2 mM L-glutamine and cyclohexamide (final concentration 100 μg/ml). Medium and cell lysate samples were collected at 0, 3, and 7 h post-chase and centrifuged at 17,000 × *g* for 10 min at 4 °C, and supernatants were transferred to fresh tubes. Collected medium was precipitated using TCA for 10 min on ice, boiled, and subjected to Western blotting.

Antibody Uptake Assay—HeLa cells grown on glass coverslips were co-transfected with the previously described GFP/CD8-CI-M6PR fusion constructs for 16 h. Transfected cells were serum-starved in DMEM supplemented with 2 mM L-glutamine for 4 h before being chased at 37 °C with anti-CD8 antibody. Post-chase coverslips were fixed in 4% PFA and subjected to indirect immunofluorescence.

Cell Surface Biotinylation—16–18 h post-transfection, transfected HeLa cells in 15-cm^2 cell culture plates were washed three times with ice-cold PBS, followed by incubation with 0.25 mg/ml EZ-link Sulfo-NHS-LC-LC Biotin (Thermo Fisher Scientific) for 10 min on ice, when reactions were quenched by 50 mM glycine for 10 min. Cells were harvested in TK lysis buffer, and protein concentrations were determined by a BCA protein quantitation assay. Equal amounts of protein lysates were incubated with Neutravidin-agarose beads (Thermo Fisher Scientific) for 1 h at 4 °C. After washing the beads three times with TK lysis buffer, beads were boiled in 2× SDS sample loading dye, and pull-down samples were subjected to SDS-PAGE/immunoblotting.

Glucose Uptake Assay—Transfected HeLa cells in a 12-well plate were washed with warmed Krebs-Ringer phosphate buffer containing 10 mM HEPES, pH 7.4, 136 mM NaCl, 4.7 mM KCl, 1.25 mM $CaCl_2$, 1.25 mM $MgSO_4$, 0.6 mM Na_2HPO_4, 0.4 mM NaH_2PO_4. Cell monolayers were incubated for 10 min in the presence of 50 μM 2-deoxy-D-glucose and 1 μCi/ml 2-deoxy-[^{3}H]glucose. The amount of glucose transported into the cells was determined by harvesting the cells in 1% Triton X-100, and the associated radioactivity was quantified using a MicroBeta liquid scintillation counter (PerkinElmer Biosciences). The counts/min were normalized to total protein concentrations.

Statistics—All statistical analyses were completed using GraphPad Prism version 6 and are described in the appropriate figure legends.

Author Contributions—J. F. performed the majority of experiments. N. A and R. G. P. contributed the EM data presented in Fig 3. S. J. N and B. M. C. contributed the ITC data presented in Fig. 1A. A. B contributed the trafficking assay presented in Fig. 7*E*. Z. Y contributed the uptake assays presented in Fig. 8, *F* and *G*. R. D. T. conceived and coordinated the study and wrote the paper with J. F. All authors reviewed the results and approved the final version of the manuscript.

Acknowledgments—We thank Stephanie Tay and Oleksiy Kovtun for assistance with protein purification. Light microscopy was carried out at the Australian Cancer Research Foundation (ACRF)/Institute for Molecular Bioscience (IMB) Dynamic Imaging Facility for Cancer Biology. We acknowledge the facilities and the scientific and technical assistance of the Australian Microscopy and Microanalysis Research Facility (AMMRF) at the Centre for Microscopy and Microanalysis (CMM), University of Queensland.

References

1. Auluck, P. K., Chan, H. Y. E., Trojanowski, J. Q., Lee, V. M.-Y., and Bonini, N. M. (2002) Chaperone suppression of α-synuclein toxicity in a *Drosophila* model for Parkinson's disease. *Science* **295,** 865–868
2. Xu, J., Kao, S. Y., Lee, F. J., Song, W., Jin, L. W., and Yankner, B. A. (2002) Dopamine-dependent neurotoxicity of α-synuclein: a mechanism for selective neurodegeneration in Parkinson disease. *Nat. Med.* **8,** 600–606
3. Emmanouilidou, E., Stefanis, L., and Vekrellis, K. (2010) Cell-produced α-synuclein oligomers are targeted to, and impair, the 26S proteasome. *Neurobiol. Aging* **31,** 953–968
4. Klein, C., and Westenberger, A. (2012) Genetics of Parkinson's disease. *Cold Spring Harb. Perspect. Med.* **2,** a008888
5. Zimprich, A., Benet-Pagès, A., Struhal, W., Graf, E., Eck, S. H., Offman, M. N., Haubenberger, D., Spielberger, S., Schulte, E. C., Lichtner, P., Rossle, S. C., Klopp, N., Wolf, E., Seppi, K., Pirker, W., *et al.* (2011) A mutation in VPS35, encoding a subunit of the retromer complex, causes late-onset Parkinson disease. *Am. J. Hum. Genet.* **89,** 168–175
6. Lesage, S., Condroyer, C., Klebe, S., Honoré, A., Tison, F., Brefel-Courbon, C., Dürr, A., Brice, A., and French Parkinson's Disease Genetics Study Group (2012) Identification of VPS35 mutations replicated in French families with Parkinson disease. *Neurology* **78,** 1449–1450
7. MacLeod, D. A., Rhinn, H., Kuwahara, T., Zolin, A., Di Paolo, G., McCabe, B. D., Marder, K. S., Honig, L. S., Clark, L. N., Small, S. A., and Abeliovich, A. (2013) RAB7L1 interacts with LRRK2 to modify intraneuronal protein sorting and Parkinson's disease risk. *Neuron* **77,** 425–439
8. Haft, C. R., de la Luz Sierra, M., Bafford, R., Lesniak, M. A., Barr, V. A., and Taylor, S. I. (2000) Human orthologs of yeast vacuolar protein sorting proteins Vps26, 29, and 35: assembly into multimeric complexes. *Mol. Biol. Cell* **11,** 4105–4116
9. Kerr, M. C., Bennetts, J. S., Simpson, F., Thomas, E. C., Flegg, C., Gleeson, P. A., Wicking, C., and Teasdale, R. D. (2005) A novel mammalian retromer component, Vps26B. *Traffic* **6,** 991–1001
10. Bugarcic, A., Zhe, Y., Kerr, M. C., Griffin, J., Collins, B. M., and Teasdale, R. D. (2011) Vps26A and Vps26B subunits define distinct retromer complexes. *Traffic* **12,** 1759–1773
11. Arighi, C. N., Hartnell, L. M., Aguilar, R. C., Haft, C. R., and Bonifacino, J. S. (2004) Role of the mammalian retromer in sorting of the cation-indepen-

dent mannose 6-phosphate receptor. *J. Cell Biol.* **165,** 123–133
12. Seaman, M. N. (2004) Cargo-selective endosomal sorting for retrieval to the Golgi requires retromer. *J. Cell Biol.* **165,** 111–122
13. Seaman, M. N. (2007) Identification of a novel conserved sorting motif required for retromer-mediated endosome-to-TGN retrieval. *J. Cell Sci.* **120,** 2378–2389
14. Seaman, M. N. (2012) The retromer complex: endosomal protein recycling and beyond. *J. Cell Sci.* **125,** 4693–4702
15. Follett, J., Bugarcic, A., Collins, B. M., and Teasdale, R. D. (2016) Retromer's role in endosomal trafficking and impaired function in neurodegenerative diseases. *Curr. Protein Pept. Sci.* 10.2174/1389203717666160311121246
16. Chi, R. J., Harrison, M. S., and Burd, C. G. (2015) Biogenesis of endosome-derived transport carriers. *Cell. Mol. Life Sci.* **72,** 3441–3455
17. Follett, J., Norwood, S. J., Hamilton, N. A., Mohan, M., Kovtun, O., Tay, S., Zhe, Y., Wood, S. A., Mellick, G. D., Silburn, P. A., Collins, B. M., Bugarcic, A., and Teasdale, R. D. (2014) The Vps35 D620N mutation linked to Parkinson's disease disrupts the cargo sorting function of retromer. *Traffic* **15,** 230–244
18. Munsie, L. N., Milnerwood, A. J., Seibler, P., Beccano-Kelly, D. A., Tatarnikov, I., Khinda, J., Volta, M., Kadgien, C., Cao, L. P., Tapia, L., Klein, C., and Farrer, M. J. (2015) Retromer-dependent neurotransmitter receptor trafficking to synapses is altered by the Parkinson's disease VPS35 mutation p.D620N. *Hum. Mol. Genet.* **24,** 1691–1703
19. McGough, I. J., Steinberg, F., Jia, D., Barbuti, P. A., McMillan, K. J., Heesom, K. J., Whone, A. L., Caldwell, M. A., Billadeau, D. D., Rosen, M. K., and Cullen, P. J. (2014) Retromer binding to FAM21 and the WASH complex is perturbed by the Parkinson disease-linked VPS35(D620N) mutation. *Curr. Biol.* **24,** 1670–1676
20. Gomez, T. S., and Billadeau, D. D. (2009) A FAM21-containing WASH complex regulates retromer-dependent sorting. *Dev. Cell* **17,** 699–711
21. Zavodszky, E., Seaman, M. N. J., Moreau, K., Jimenez-Sanchez, M., Breusegem, S. Y., Harbour, M. E., and Rubinsztein, D. C. (2014) Mutation in VPS35 associated with Parkinson's disease impairs WASH complex association and inhibits autophagy. *Nat. Commun.* **5,** 3828
22. Hierro, A., Rojas, A. L., Rojas, R., Murthy, N., Effantin, G., Kajava, A. V., Steven, A. C., Bonifacino, J. S., and Hurley, J. H. (2007) Functional architecture of the retromer cargo-recognition complex. *Nature* **449,** 1063–1067
23. Ariotti, N., Hall, T. E., Rae, J., Ferguson, C., McMahon, K.-A., Martel, N., Webb, R. E., Webb, R. I., Teasdale, R. D., and Parton, R. G. (2015) Modular detection of GFP-labeled proteins for rapid screening by electron microscopy in cells and organisms. *Dev. Cell* **35,** 513–525
24. Seaman, M. N. J., Harbour, M. E., Tattersall, D., Read, E., and Bright, N. (2009) Membrane recruitment of the cargo-selective retromer subcomplex is catalysed by the small GTPase Rab7 and inhibited by the Rab-GAP TBC1D5. *J. Cell Sci.* **122,** 2371–2382
25. Harbour, M. E., Breusegem, S. Y., Antrobus, R., Freeman, C., Reid, E., and Seaman, M. N. (2010) The cargo-selective retromer complex is a recruiting hub for protein complexes that regulate endosomal tubule dynamics. *J. Cell Sci.* **123,** 3703–3717
26. Harbour, M. E., Breusegem, S. Y., and Seaman, M. N. (2012) Recruitment of the endosomal WASH complex is mediated by the extended "tail" of Fam21 binding to the retromer protein Vps35. *Biochem. J.* **442,** 209–220
27. Jia, D., Gomez, T. S., Billadeau, D. D., and Rosen, M. K. (2012) Multiple repeat elements within the FAM21 tail link the WASH actin regulatory complex to the retromer. *Mol. Biol. Cell* **23,** 2352–2361
28. Mecozzi, V. J., Berman, D. E., Simoes, S., Vetanovetz, C., Awal, M. R., Patel, V. M., Schneider, R. T., Petsko, G. A., Ringe, D., and Small, S. A. (2014) Pharmacological chaperones stabilize retromer to limit APP processing. *Nat. Chem. Biol.* **10,** 443–449
29. Cuervo, A. M., Stefanis, L., Fredenburg, R., Lansbury, P. T., and Sulzer, D. (2004) Impaired degradation of mutant α-synuclein by chaperone-mediated autophagy. *Science* **305,** 1292–1295
30. Cullen, V., Lindfors, M., Ng, J., Paetau, A., Swinton, E., Kolodziej, P., Boston, H., Saftig, P., Woulfe, J., Feany, M. B., Myllykangas, L., Schlossmacher, M. G., and Tyynelä, J. (2009) Cathepsin D expression level affects α-synuclein processing, aggregation, and toxicity *in vivo*. *Mol. Brain* **2,** 5
31. Follett, J., Darlow, B., Wong, M. B., Goodwin, J., and Pountney, D. L. (2013) Potassium depolarization and raised calcium induces α-synuclein aggregates. *Neurotox. Res.* **23,** 378–392
32. Tanik, S. A., Schultheiss, C. E., Volpicelli-Daley, L. A., Brunden, K. R., and Lee, V. M. (2013) Lewy body-like α-synuclein aggregates resist degradation and impair macroautophagy. *J. Biol. Chem.* **288,** 15194–15210
33. Decressac, M., Mattsson, B., Weikop, P., Lundblad, M., Jakobsson, J., and Björklund, A. (2013) TFEB-mediated autophagy rescues midbrain dopamine neurons from α-synuclein toxicity. *Proc. Natl. Acad. Sci. U.S.A.* **110,** E1817–E1826
34. Konno, M., Hasegawa, T., Baba, T., Miura, E., Sugeno, N., Kikuchi, A., Fiesel, F. C., Sasaki, T., Aoki, M., Itoyama, Y., and Takeda, A. (2012) Suppression of dynamin GTPase decreases α-synuclein uptake by neuronal and oligodendroglial cells: a potent therapeutic target for synucleinopathy. *Mol. Neurodegener.* **7,** 38
35. Temkin, P., Lauffer, B., Jäger, S., Cimermancic, P., Krogan, N. J., and von Zastrow, M. (2011) SNX27 mediates retromer tubule entry and endosome-to-plasma membrane trafficking of signalling receptors. *Nat. Cell Biol.* **13,** 715–721
36. Steinberg, F., Gallon, M., Winfield, M., Thomas, E. C., Bell, A. J., Heesom, K. J., Tavaré, J. M., and Cullen, P. J. (2013) A global analysis of SNX27-retromer assembly and cargo specificity reveals a function in glucose and metal ion transport. *Nat. Cell Biol.* **15,** 461–471
37. Gallon, M., Clairfeuille, T., Steinberg, F., Mas, C., Ghai, R., Sessions, R. B., Teasdale, R. D., Collins, B. M., and Cullen, P. J. (2014) A unique PDZ domain and arrestin-like fold interaction reveals mechanistic details of endocytic recycling by SNX27-retromer. *Proc. Natl. Acad. Sci. U.S.A.* **111,** E3604–E3613
38. Popovic, D., Akutsu, M., Novak, I., Harper, J. W., Behrends, C., and Dikic, I. (2012) Rab GTPase-activating proteins in autophagy: regulation of endocytic and autophagy pathways by direct binding to human ATG8 modifiers. *Mol. Cell. Biol.* **32,** 1733–1744
39. Hong, Z., Yang, Y., Zhang, C., Niu, Y., Li, K., Zhao, X., and Liu, J. J. (2009) The retromer component SNX6 interacts with dynactin p150(Glued) and mediates endosome-to-TGN transport. *Cell Res.* **19,** 1334–1349
40. Harrison, M. S., Hung, C.-S., Liu, T.-T., Christiano, R., Walther, T. C., and Burd, C. G. (2014) A mechanism for retromer endosomal coat complex assembly with cargo. *Proc. Natl. Acad. Sci. U.S.A.* **111,** 267–272
41. Priya, A., Kalaidzidis, I. V., Kalaidzidis, Y., Lambright, D., and Datta, S. (2015) Molecular insights into Rab7-mediated endosomal recruitment of core retromer: deciphering the role of Vps26 and Vps35. *Traffic* **16,** 68–84
42. Hossain, S., Alim, A., Takeda, K., Kaji, H., Shinoda, T., and Uéda, K. (2001) Limited proteolysis of NACP/α-synuclein. *J. Alzheimers Dis.* **3,** 577–584
43. Sevlever, D., Jiang, P., and Yen, S. H. (2008) Cathepsin D is the main lysosomal enzyme involved in the degradation of α-synuclein and generation of its carboxy-terminally truncated species. *Biochemistry* **47,** 9678–9687
44. Miura, E., Hasegawa, T., Konno, M., Suzuki, M., Sugeno, N., Fujikake, N., Geisler, S., Tabuchi, M., Oshima, R., Kikuchi, A., Baba, T., Wada, K., Nagai, Y., Takeda, A., and Aoki, M. (2014) VPS35 dysfunction impairs lysosomal degradation of α-synuclein and exacerbates neurotoxicity in a *Drosophila* model of Parkinson's disease. *Neurobiol. Dis.* **71,** 1–13
45. Cuervo, A. M., and Dice, J. F. (2000) Age-related decline in chaperone-mediated autophagy. *J. Biol. Chem.* **275,** 31505–31513
46. Li, N., Ragheb, K., Lawler, G., Sturgis, J., Rajwa, B., Melendez, J. A., and Robinson, J. P. (2003) Mitochondrial complex I inhibitor rotenone induces apoptosis through enhancing mitochondrial reactive oxygen species production. *J. Biol. Chem.* **278,** 8516–8525
47. Yoshimori, T., Yamamoto, A., Moriyama, Y., Futai, M., and Tashiro, Y. (1991) Bafilomycin A1, a specific inhibitor of vacuolar-type H^+-ATPase, inhibits acidification and protein degradation in lysosomes of cultured cells. *J. Biol. Chem.* **266,** 17707–17712
48. Jäger, S., Bucci, C., Tanida, I., Ueno, T., Kominami, E., Saftig, P., and Eskelinen, E.-L. (2004) Role for Rab7 in maturation of late autophagic vacuoles. *J. Cell Sci.* **117,** 4837–4848
49. Popovic, D., and Dikic, I. (2014) TBC1D5 and the AP2 complex regulate ATG9 trafficking and initiation of autophagy. *EMBO Rep.* **15,** 392–401
50. Rojas, R., van Vlijmen, T., Mardones, G. A., Prabhu, Y., Rojas, A. L., Mohammed, S., Heck, A. J. R., Raposo, G., van der Sluijs, P., and Bonifacino,

J. S. (2008) Regulation of retromer recruitment to endosomes by sequential action of Rab5 and Rab7. *J. Cell Biol.* **183,** 513–526
51. Norwood, S. J., Shaw, D. J., Cowieson, N. P., Owen, D. J., Teasdale, R. D., and Collins, B. M. (2011) Assembly and solution structure of the core retromer protein complex. *Traffic* **12,** 56–71
52. Furlong, R. A., Narain, Y., Rankin, J., Wyttenbach, A., and Rubinsztein, D. C. (2000) α-Synuclein overexpression promotes aggregation of mutant huntingtin. *Biochem. J.* **346,** 577–581
53. Lee, H. J., Shin, S. Y., Choi, C., Lee, Y. H., and Lee, S. J. (2002) Formation and removal of α-synuclein aggregates in cells exposed to mitochondrial inhibitors. *J. Biol. Chem.* **277,** 5411–5417
54. Scotter, E. L., Vance, C., Nishimura, A. L., Lee, Y. B., Chen, H. J., Urwin, H., Sardone, V., Mitchell, J. C., Rogelj, B., Rubinsztein, D. C., and Shaw, C. E. (2014) Differential roles of the ubiquitin proteasome system and autophagy in the clearance of soluble and aggregated TDP-43 species. *J. Cell Sci.* **127,** 1263–1278

Parkinson Disease-linked Vps35 R524W Mutation Impairs the Endosomal Association of Retromer and Induces α-Synuclein Aggregation

Jordan Follett, Andrea Bugarcic, Zhe Yang, Nicholas Ariotti, Suzanne J. Norwood, Brett M. Collins, Robert G. Parton and Rohan D. Teasdale

J. Biol. Chem. 2016, 291:18283-18298.
doi: 10.1074/jbc.M115.703157 originally published online July 6, 2016